Ab Initio Study on Luminescent Properties and Aurophilic Attraction of [Au_2(dpm)(i-mnt)] and Its Related Au(I) Complexes (dpm = bis(diphosphino)methane and i-mnt = i-malononitriledithiolate)

Qing-Jiang Pan and Hong-Xing Zhang*

State Key Laboratory of Theoretical and Computational Chemistry, Institute of Theoretical Chemistry, Jilin University, Changchun 130023, People's Republic of China

Received February 25, 2004

The ground- and excited-state properties of the model compound [Au_2(dpm)(i-mnt)] (**1**) (dpm = bis(diphosphino)methane and i-mnt = i-malononitriledithiolate) are studied by ab initio methods. The calculated Au−Au distance (2.913 Å) and the corresponding Au−Au stretching frequency (110 cm^{-1}) in the $^1A'$ ground state at the MP2 level indicate the existence of weak aurophilic attraction in the compound. Four excited states of **1** producing the emissions in the gas phase are obtained by CIS calculations. The IPCM model and the dimerization model, [Au_2(dpm)(i-mnt)]$_2$ (**1**···**1**), are employed to account for the solvent and solid effects, respectively. The 454 nm emission from the $b^3A''\rightarrow{}^1A'$ transition is assigned as an Au−Au→S charge transfer (^{3}MMLCT) transition, and the interaction between the σ/π-(Au_2) and π(i-mnt) orbitals rationalizes the much longer Au−Au distance (3.467 Å) in the b^3A'' excited state. The c^3A' excited state gives the 307 nm emission in the gas phase and the 512 nm emission in acetonitrile, both with the character of the Au−Au→i-mnt charge transfer, where the latter is comparable to experimental 558 nm emission of [Au_2(dmpm)-(i-mnt)] (dmpm = bis(dimethylphosphino)methane) in acetonitrile. The calculated absorptions of **1** in acetonitrile agree well with experimental observations. The comparison between **1** and related Au(I) complexes ([Au_2(dpm)$_2$]$^{2+}$ (**2**), [$Au_2(PH_3)_2$(i-mnt)] (**3**), and [Au_2(dpm)(SCH_2S)] (**4**)) contributes to the understanding of the luminescence and aurophilicity of these Au(I) complexes.

I. Introduction

The luminescent properties and aurophilic attraction in Au(I) complexes and the relationship between them have been paid great attention in the last two decades.[1−10] The energy of Au^I−Au^I aurophilic attraction existing in the solid state and solution is estimated to be 30−60 kJ/mol,[4,8c,11] comparable to that of hydrogen bonds. For the case of intramolecular interactions, the presence of bridging ligands facilitates intramolecular aurophilic contacts in bi- or polynuclear complexes, which has been illustrated by complexes [Au_2(dithiolate)$_2$], [Au_2(diphosphine)(dithiolate)], and [Au_2-(diphosphine)$_2$], where the Au^I−Au^I distances are about 2.8−3.0 Å.[12−14] Such a short distance indicates significant aurophilic attraction between the two Au(I) atoms, by considering the much shorter Au^I−Au^I distance than the van der Waals contacts of 3.4 Å.[15] Pyykkö and coworkers have attributed the attraction to correlation effects, strengthened by relativistic effects.[4]

The Au(I) complexes are usually luminescent, especially when aurophilic attraction is present.[1,6−10,16−19] The assignment of the emitting state has been a matter of some discussion. The emission of several binuclear phosphine Au(I) complexes was assigned to metal-

(1) (a) Lee, Y. A.; McGarrah, J. E.; Lachicotte, R. J.; Eisenberg, R. *J. Am. Chem. Soc.* **2002**, *124*, 10662. (b) Mansour, M. A.; Connick, W. B.; Lachicotte, R. J.; Gysling, H. J.; Eisenberg, R. *J. Am. Chem. Soc.* **1998**, *120*, 1329. (c) Hao, L.; Lachicotte, R. J.; Gysling, H. J.; Eisenberg, R. *Inorg. Chem.* **1999**, *38*, 4616.

(2) (a) White-Morris, R. L.; Olmstead, M. M.; Balch, A. L. *J. Am. Chem. Soc.* **2003**, *125*, 1033. (b) White-Morris, R. L.; Olmstead, M. M.; Jiang, F.; Tinti, D. S.; Balch, A. L. *J. Am. Chem. Soc.* **2002**, *124*, 2327. (c) Olmsted, M. M.; Jiang, F.; Attar, S.; Balch, A. L. *J. Am. Chem. Soc.* **2001**, *123*, 3260. (d) White-Morris, R. L.; Stender, M.; Tinti, D. S.; Balch, A. L. *Inorg. Chem.* **2003**, *42*, 3237. (e) White-Morris, R. L.; Olmstead, M. M.; Jiang, F.; Balch, A. L. *Inorg. Chem.* **2002**, *41*, 2313. (f) Calcar, P. M. V.; Olmstead, M. M.; Balch, A. L. *Inorg. Chem.* **1997**, *36*, 5231. (g) Weissbart, B.; Toronto, D. V.; Balch, A. L.; Tinti, D. S. *Inorg. Chem.* **1996**, *35*, 2490. (h) Toronto, D. V.; Weissbart, B.; Tinti, D. S.; Balch, A. L. *Inorg. Chem.* **1996**, *35*, 2484. (i) Vickery, J. C.; Lomstead, M. M.; Fung, E. Y.; Balch, A. L. *Angew. Chem., Int. Ed.* **1997**, *36*, 1179.

(3) (a) Gimeno, M. C.; Laguna, A. *Chem. Rev.* **1997**, *97*, 511. (b) Crespo, O.; Gimeno, M. C.; Jones, P. G.; Laguna, A.; López-de-Luzuraga, J. M.; Monge, M.; Pérez, J. L.; Ramón, M. A. *Inorg. Chem.* **2003**, *42*, 2061. (c) Bardají, M.; Laguna, A.; Jones, P. G.; Fischer, A. K. *Inorg. Chem.* **2000**, *39*, 3560. (d) Bardají, M.; Laguna, A.; Orera, V. M.; Villacampa, M. D. *Inorg. Chem.* **1998**, *37*, 5125. (e) Fernández, E. J.; López-de-Luzuraga, J. M.; Monge, M.; Rodríguez, M. A.; Crespo, O.; Gimeno, M. C.; Laguna, A.; Jones, P. G. *Inorg. Chem.* **1998**, *37*, 6002. (f) Gimeno, M. C.; Jones, P. G.; Laguna, A.; Laguna, M.; Terrobal, R. *Inorg. Chem.* **1994**, *33*, 3932. (g) Fernández, E. J.; López-de-Luzuriaga, J. M.; Monge, M.; Rodríguez, M. A.; Crespo, O.; Gimeno, M. C.; Laguna, A.; Jones, P. G. *Chem. Eur. J.* **2000**, *6*, 636. (h) Gimeno, M. C.; Jones, P. G.; Laguna, A.; Sarroca, C.; Calhorda, M. J.; Veiros, L. F. *Chem. Eur. J.* **1998**, *4*, 2308. (i) Bardají, M.; Laguna, A.; Pérez, M. R. *Organometallics* **2002**, *21*, 1877. (j) Codina, A.; Fernández, E. J.; Jones, P. G.; Laguna, A.; López-de-Luzuriaga, J. M.; Monge, M.; Olmos, M. E.; Pérez, J.; Rodríguez, M. A. *J. Am. Chem. Soc.* **2002**, *124*, 6781.

10.1021/om0498652 CCC: $27.50
Publication on Web 09/14/2004

centered (MC) transitions.[7] In several binuclear Au(I) phosphine thiolate complexes, however, the emission was attributed to the Au to thiolate or sulfur charge transfer (MLCT) transition.[8b,10,12,17]

In binuclear Au(I) complexes, phosphines differ from thiolates in bonding nature.[20,21] Phosphine ligands provide lone pair electrons to contribute the dative bond from P to Au; however, thiolates, as anions, prefer the covalent bonding between the S and Au atoms to coordinating. These different electronic properties will change the luminescent properties when thiolates are introduced into the phosphine Au(I) complexes, [Au$_2$(diphosphine)$_2$], to form Au(I) phosphine thiolate complexes, [Au$_2$(diphosphine)(dithiolate)].[21] Recently, we have used ab initio methods to investigate the spectroscopic properties and electronic structures of [Au$_2$(dpm)$_2$]$^{2+}$ (**2**),[21a] [Au$_2$(PH$_3$)$_2$(i-mnt)] (**3**),[21c] and [Au$_2$(dpm)(SCH$_2$S)] (**4**)[21b] (dpm = bis(diphosphino)methane and i-mnt = i-malononitriledithiolate) to reveal electron transition characteristics during the absorption and emission processes in solid state and solution, which agree well with previous experimental observations.[7,8bc,10a,17] We rectified the transition property of the 462 nm solid-state emission of [Au$_2$(PPh$_3$)$_2$(i-mnt)] from ^{3}MLCT assigned by Zink et al.[10a] to ^{3}MMLCT because of the presence of the stronger Au−Au bonding in the emissive excited state of **3**.[21c]

Recently, Tang and co-workers[12] have reported that complexes [Au$_2$(P−P)(i-mnt)] (P−P = dmpm, dppm, dmpe, and dppe) (dmpm = bis(dimethylphosphino)methane, dppm = bis(diphenylphosphino)methane, dmpe = bis(dimethylphosphino)ethane, and dppe = bis(diphenylphosphino)ethane) exhibit an intense phosphorescent emission in the range 540−576 nm in acetonitrile at 77 K which was experimentally attributed to the ^{3}MLCT transition from the triplet excited state to the singlet ground state. As a π-conjugated thiolate ligand, i-mnt is greatly involved in the emission process of such complexes, which is also supported by many luminescent complexes containing the ligand such as K$_2$(i-mnt), [(n-Bu)$_4$N]$_2$[M(i-mnt)$_2$] (M = Cu, Ni, Pd, and Pt), and [Au$_2$(PPh$_3$)$_2$(i-mnt)].[10,12,22] The structural characterization from X-ray crystal diffraction shows that the [Au$_2$(dmpm)(i-mnt)] complex forms polymers through the intermolecular Au−Au interactions and has a rather short intramolecular Au^I−Au^I distance of 2.909 Å.[12] Since the Au(I) complex possesses both Au−Au interactions and luminescence, it can serve as an ideal candidate to study the relationship between them. Moreover, the studies on the model complex [Au$_2$(dpm)(i-mnt)] (**1**), representing [Au$_2$(dmpm)(i-mnt)] and [Au$_2$(dppm)(i-mnt)], are of importance in both theory and experiment. First, the systematic studies on **1**−**4** can perfect the theoretical works on the excited-state properties of a series of Au(I) complexes[21] and explore the application of the theoretical methods in the transition metal complexes.[23] The comparison of **1** and **2** helps us further understand what effect the introduction of the thiolate ligand (i-mnt) has on excited-state properties of the Au(I) complexes; the investigations on **1** and **3** can specify the differences in luminescent properties of the open- and closed-ring Au(I) complexes; the comparison between **1** and **4** rationalizes the influence of the π-conjugated ligand on the transition properties and excited-state structures of Au(I) complexes. Second, the studies

(4) (a) Pyykkö, P.; Runeberg, N.; Mendizabal, F. *Chem. Eur. J.* **1997**, *3*, 1451. (b) Pyykkö, P.; Mendizabal, F. *Chem. Eur. J.* **1997**, *3*, 1458. (c) Pyykkö, P.; Mendizabal, F. *Inorg. Chem.* **1998**, *37*, 3018. (d) Pyykkö, P. *Chem. Rev.* **1997**, *97*, 597. (e) Pyykkö, P. *Chem. Rev.* **1988**, *88*, 563. (f) Pyykkö, P.; Schneider, W.; Bauer, A.; Bayler, A.; Schmidbaur, H. *Chem. Commun.* **1997**, 1111. (g) Pyykkö, P.; Zhao, Y.-F. *Angew. Chem., Int. Ed.* **1991**, *30*, 604; *Angew. Chem.* **1991**, *103*, 622. (h) Li, J.; Pyykkö, P. *Chem. Phys. Lett.* **1992**, *197*, 586. (i) Pyykkö, P.; Li, J.; Runeberg, N. *Chem. Phys. Lett.* **1994**, *218*, 133. (j) Li, J.; Pyykkö, P. *Inorg. Chem.* **1993**, *32*, 2630.

(5) (a) Forward, J. M.; Assefa, Z.; Facker, J. P., Jr. *J. Am. Chem. Soc.* **1995**, *177*, 9103. (b) Forward, J. M.; Assefa, Z.; Staples, R. J.; Fackler, J. P., Jr. *Inorg. Chem.* **1996**, *35*, 16. (c) Assefa, Z.; McBurnett, B. G.; Staples, R. J.; Fackler, J. P., Jr. *Inorg. Chem.* **1995**, *34*, 75. (d) Assefa, Z.; McBurnett, B. G.; Staples, R. J.; Fackler, J. P., Jr. *Inorg. Chem.* **1995**, *34*, 4965. (e) Dávila, R. M.; Elduque, A.; Grant, T.; Staples, R. J.; Fackler, J. P., Jr. *Inorg. Chem.* **1993**, *32*, 1749. (f) King, C.; Khan, M. N. I.; Staples, R. J.; Fackler, J. P., Jr. *Inorg. Chem.* **1992**, *31*, 3236. (g) Wang, S.; Garzón, G.; King, C.; Wang, J. C.; Fackler, J. P., Jr. *Inorg. Chem.* **1989**, *28*, 4623. (h) Khan, Md. N. I.; King, C.; Heinrich, D. D.; Fackler, J. P., Jr.; Porter, L. C. *Inorg. Chem.* **1989**, *28*, 2150. (i) Khan, Md. N. I.; Wang, S.; Fackler, J. P., Jr. *Inorg. Chem.* **1989**, *28*, 3579.

(6) (a) Lu, W.; Xiang, H.-F.; Zhu, N.; Che, C.-M. *Organometallics* **2002**, *21*, 2343. (b) Che, C.-M.; Chao, H.-Y.; Miskowski, V. M.; Li, Y.; Cheung, K.-K. *J. Am. Chem. Soc.* **2001**, *123*, 4985. (c) Che, C.-M.; Wong, W.-T.; Lai, T.-F.; Kwong, H.-L. *J. Chem. Soc., Chem. Commun.* **1989**, 243. (d) Lu, W.; Zhu, N.; Che, C.-M. *J. Organomet. Chem.* **2003**, *670*, 11.

(7) (a) Leung, K. H.; Phillips, D. L.; Tse, M.-C.; Che, C.-M.; Miskowski, V. M. *J. Am. Chem. Soc.* **1999**, *121*, 4799. (b) Fu, W.-F.; Chan, K.-C.; Miskowski, V. M.; Che, C.-M. *Angew. Chem. Int. Ed.* **1999**, *38*, 2783. (c) Che, C.-M.; Kwong, H.-L.; Yam, V. W.-W.; Cho, K.-C. *J. Chem. Soc., Chem. Commun.* **1989**, 885. (d) Che, C.-M.; Kwong, H.-L.; Poon, C.-K. *J. Chem. Soc., Dalton Trans.* **1990**, 3215.

(8) (a) Schwerdtfeger, P.; Bruce, A. E.; Bruce, M. R. M. *J. Am. Chem. Soc.* **1998**, *120*, 6587. (b) Jones, W. B.; Yuan, J.; Narayanaswamy, R.; Young, M. A.; Elder, R. C.; Bruce, A. E.; Bruce, M. R. M. *Inorg. Chem.* **1995**, *34*, 1996. (c) Narayanaswamy, R.; Young, M. A.; Parkhurst, E.; Ouellette, M.; Kerr, M. E.; Ho, K. M.; Elder, R. C.; Bruce, A. E.; Bruce, M. R. M. *Inorg. Chem.* **1993**, *32*, 2506.

(9) (a) Yam, V. W.-W.; Lo, K. K. W. *Chem. Soc. Rev.* **1999**, *28*, 323. (b) Yam, V. W.-W.; Cheng, E. C.-C.; Zhou, Z.-Y. *Angew. Chem., Int. Ed.* **2000**, *39*, 1683. (c) Yam, V. W.-W.; Li, C.-K.; Chan, C.-L. *Angew. Chem., Int. Ed.* **1998**, *37*, 2857. (d) Yam, V. W.-W.; Lai, T.-F.; Che, C.-M. *J. Chem. Soc., Dalton Trans.* **1990**, 3747.

(10) (a) Hanna, S. D.; Zink, J. I. *Inorg. Chem.* **1996**, *35*, 297. (b) Hanna, S. D.; Khan, S. I.; Zink, J. I. *Inorg. Chem.* **1996**, *35*, 5813.

(11) Pathaneni, S. S.; Desiraju, G. R. *J. Chem. Soc., Dalton Trans.* **1993**, 319.

(12) Tang, S. S.; Chang, C.-P.; Lin, I. J. B.; Liou, L.-S. Wang, J.-C. *Inorg. Chem.* **1997**, *36*, 2294.

(13) (a) Schaefer, W. P.; Marsh, R. E.; McCleskey, T. M.; Gray, H. B. *Acta Crystallogr.* **1991**, *C47*, 2553. (b) Porter, L. C.; Khan, Md. N. I.; King, C.; Fackler, J. P., Jr. *Acta Crystallogr.* **1989**, *C45*, 947. (c) Wang, J.-C.; Khan, Md. N. I.; Fackler, J. P., Jr. *Acta Crystallogr.* **1989**, *C45*, 1482. (d) Kozelka, J.; Oswald, H. R.; Dubler, E. *Acta Crystallogr.* **1986**, *C42*, 1007. (e) Briant, C. E.; Hall, K. P.; Mingos, D. M. P. *J. Organomet. Chem.* **1982**, *229*, C5. (f) Shain, J.; Fackler, J. P., Jr. *Inorg. Chim. Acta* **1987**, *131*, 157. (g) Payne, N. C.; Puddephatt, R. J.; Ravindranath, R.; Treurnicht, I. *Can. J. Chem.* **1988**, *66*, 3176.

(14) (a) Heinrich, D. D.; Wang, J.-C.; Fackler, J. P., Jr. *Acta Crystallogr.* **1990**, *C46*, 1444. (b) Khan, Md. N. I.; Wang, S.; Heinrich, D. D.; Fackler, J. P., Jr. *Acta Crystallogr.* **1988**, *C44*, 822. (c) Hesse, R.; Jennische, P. *Acta Chem. Scand.* **1972**, *26*, 3855.

(15) Bondi, A. *J. Phys. Chem.* **1964**, *68*, 441.

(16) Bachman, R. E.; Bodolosky-Bettis, S. A.; Glennon, S. C.; Sirchio, S. A. *J. Am. Chem. Soc.* **2000**, *122*, 7146.

(17) King, C.; Wang, J.-C.; Khan, M. N. I.; Fackler, J. P., Jr. *Inorg. Chem.* **1989**, *28*, 2145.

(18) Khan, Md. N. I.; Fackler, J. P., Jr.; King, C.; Wang, J. C.; Wang, S. *Inorg. Chem.* **1988**, *27*, 1672.

(19) Forward, J. M.; Bohmann, D.; Fackler, J. P., Jr.; Staples, R. J. *Inorg. Chem.* **1995**, *34*, 6330.

(20) (a) Schwerdtfeger, P.; Hermann, H. L.; Schmidbaur, H. *Inorg. Chem.* **2003**, *42*, 1334. (b) Römbke, P.; Schier, A.; Wiesbrock, F.; Schmidbaur, H. *Inorg. Chim. Acta* **2003**, *347*, 123. (c) Rodriguez, J. A.; Dvorak, J.; Jirsak, T.; Liu, G.; Hrbek, J.; Aray, Y.; González, C. *J. Am. Chem. Soc.* **2003**, *125*, 276. (d) Bowmaker, B. A.; Schmidbaur, H.; Krüger, S.; Rösch, N. *Inorg. Chem.* **1997**, *36*, 1754. (e) Kichkelbick, G.; Schubert, U. *Inorg. Chim. Acta* **1997**, *262*, 61.

(21) (a) Zhang, H.-X.; Che, C.-M. *Chem. Eur. J.* **2001**, *7*, 4887. (b) Pan, Q.-J.; Zhang, H.-X. *J. Chem. Phys.* **2003**, *119*, 4346. (c) Pan, Q.-J.; Zhang, H.-X. *Eur. J. Inorg. Chem.* **2003**, 4202. (d) Pan, Q.-J.; Zhang, H.-X. *Inorg. Chem.* **2004**, *43*, 593. (e) Pan, Q.-J.; Zhang, H.-X. *J. Phys. Chem. A* **2004**, *108*, 3650.

(22) Werden, B. G.; Billig, E.; Gray, H. B. *Inorg. Chem.* **1966**, *5*, 78.

(23) Halls, M. D.; Schlegel, H. B. *Chem. Mater.* **2001**, *13*, 2632.

on **1**−**4** provide the support in theory for experimental observations, especially for the existing and/or potential applications of Au(I) complexes.[1,7,9a,24]

Here, the ab initio methods are employed to study the spectroscopic properties and electronic structures of complex **1** in the gas phase and solution. The solvent effect of acetonitrile is taken into account with the isodensity polarized continuum model (IPCM)[25−27] in the self-consistent reaction field (SCRF) method. In our calculations, the 672, 454, 307, and 301 nm emissions in the gas phase and 716, 624, 512, and 375 nm emissions in acetonitrile arising from $a^3A' \rightarrow {}^1A'$, $b^3A'' \rightarrow {}^1A'$, $c^3A' \rightarrow {}^1A'$, and ${}^1A'' \rightarrow {}^1A'$ transitions are assigned as i-mnt intraligand charge transfer (^{3}ILCT), Au−Au→S charge transfer (^{3}MMLCT), Au−Au→i-mnt charge transfer (^{3}MMLCT), and $Au((sp)_\sigma) \rightarrow Au(d_{\sigma^*})$ (^{1}MC) transition, respectively. On the basis of the optimized c^3A' excited-state structure, the dimer, $[Au_2(dpm)(i\text{-}mnt)]_2$ (**1**···**1**), is used to simulate the behavior of **1** in the solid state. The results indicate the solid effect slightly changes the emission of complex **1**. The detailed comparison among **1**−**4** provides deep insight into the nature of the luminescence and aurophilicity of these Au(I) complexes.

II. Computational Details and Theory

In the calculations, we use $[Au_2(dpm)(i\text{-}mnt)]$ (**1**) as the computational model to represent real complex $[Au_2(P-P)(i\text{-}mnt)]$ (P−P = dmpm and dppm). A similar model was applied in our previous work[21a] by using dpm to stand for dmpm, dppm, and dcpm in the $[Au_2(dmpm)_2]^{2+}$, $[Au_2(dppm)_2]^{2+}$, and $[Au_2(dcpm)_2]^{2+}$ (dcpm = bis(dicyclohexylphosphino)-methane) complexes, respectively. It is a general technique to employ hydrogen to substitute methyl, phenyl, and other heavy substituents in ab initio studies to save computational resources. Häberlen and Rösch[28] have proved that PH_3 provides a satisfactory model of the full PMe_3 or PPh_3 for structural properties of Au(I) complexes. Fackler[17] and other researchers[8a,20a,29−30] have successfully used such a model in their theoretical studies on related topics of phosphine Au(I) complexes.

In this work, C_s symmetry is adopted to settle the conformation of **1** in both the ground and excited states, which is consistent with the data of X-ray diffraction of $[Au_2(dmpm)(i\text{-}mnt)]$.[12] The structure of the ground state is fully optimized at the second-order Møller−Plesset perturbation (MP2)[31] level, while the structure of the excited state is optimized by the single excitation configuration interaction (CIS)[32] method to reveal the luminescent properties. On the basis of such calculations, IPCM in the SCRF method[25−27] is employed to account for solvent effects of acetonitrile, by considering the dramatic red shift of emission due to the solvation of acetonitrile on **2** indicated in the previous work.[21a] Therefore, the electronic structures of the excited state and the absorption and emission in acetonitrile are obtained. As a reference, the absorption and emission of the i-mnt ligand are studied using the same methods and basis sets as those of **1**. The ligand also keeps the C_s symmetry in the calculations of the ground and excited states.

In principle, the calculation on the single **1** molecule corresponds to the properties of the molecule in the gas phase.[33] In crystalline form, the dimer of $[Au_2(dmpm)(i\text{-}mnt)]$ connected by the intermolecular Au−Au interaction forms a repeated unit, and many such units aggregate the polymer.[12] Thus, we use the $[Au_2(dpm)(i\text{-}mnt)]_2$ model (**1**···**1**) to simulate the behavior of the Au(I) complex in the solid state. It has been reported that the complex $[Au_2(dmpm)(i\text{-}mnt)]$ exhibits an intense 558 nm phosphorescent emission in acetonitrile at 77 K, experimentally assigned as an Au→i-mnt charge transfer.[12] As the temperature decreases, the Au−Au interaction increases.[34] So both solvent and solid effects have to be considered in the calculations to describe the behavior of the emission in solution at lower temperature. Because of the expensive computational cost for **1**···**1**, we discuss only how the solid effect affects the emission with the character of the Au→i-mnt charge transfer.

In the calculations, quasi-relativistic pseudopotentials of the Au, S, and P atoms proposed by Hay and Wadt[35] with 19, 6, and 5 valence electrons, respectively, are employed and the LanL2DZ basis sets associated with the pseudopotential are adopted and implemented by one additional f-type function for Au ($\alpha_f = 0.2$) and d-type function for S ($\alpha_d = 0.4210$) and P ($\alpha_d = 0.34$).[4,21b−d] It has been found that the f-type polarization functions are required for precisely describing the aurophilic interaction[4a−c] and the potential energy surface of the excited states.[32a] In S-Table 1 (Supporting Information), the comparison among basis sets without and with one and two f-type polarization functions on Au atoms in the optimized ground-state geometries for **1** indicates that the introduction of the polarization functions is important to describe the Au−Au aurophilic attraction and the results from one f-function addition to the Au atom are very close to experimental values.[12] To save computational resources, we add only one f function to the Au atom in the present calculations. The basis sets are taken as Au(8s6p3d1f/3s3p2d1f), S(3s3p1d/2s2p1d), P(3s3p1d/2s2p1d), N(10s5p/3s2p), C(10s5p/3s2p), and H(4s/2s). Thus, 185 basis functions and 110 electrons are included for **1** in

(24) (a) McKeage, M. J.; Maharaj, L.; Berners-Price, S. J. *Coord. Chem. Rev.* **2002**, *232*, 127. (b) Berners-Price, S. J.; Bowen, R. J.; Galettis, P.; Healy, P. C.; McKeage, M. J. *Coord. Chem. Rev.* **1999**, *185*−*186*, 823. (c) Navarro, M.; Pérez, H.; Sánchez-Delgado, R. A. *J. Med. Chem.* **1997**, *40*, 1937. (d) Berners-Price, S. J.; Girard, G. R.; Hill, D. T.; Sutton, B. M.; Jarrett, P. S.; Faucette, L. F.; Johnson, R. K.; Mirabelli, C. K.; Sadler, P. J. *J. Med. Chem.* **1990**, *33*, 1386. (e) Corey, E. J.; Mahrotra, M. M.; Khan, A. U. *Science* **1987**, *236*, 68. (f) Mirabelli, C. K.; Johnson, R. K.; Hill, D. T.; Faucette, L. F.; Girard, G. R.; Kuo, G. Y.; Sung, C. M.; Crooke, S. T. *J. Med. Chem.* **1986**, *29*, 218. (g) Weinstock, J.; Sutton, B. M.; Kuo, G. Y.; Walz, D. T.; Dimartino, M. J. *J. Med. Chem.* **1974**, *17*, 139.

(25) Sanscores, L. E.; Salcedo, R.; Flores, H.; Martinez, A. *J. Mol. Struct. (THEOCHEM)* **2000**, *530*, 125.

(26) Foresman, J. B.; Keith, T. A.; Wiberg, K. B.; Snoonian, J.; Frisch, M. J. *J. Phys. Chem.* **1996**, *100*, 16098.

(27) Frisch, M. J.; Trucks, G. W.; Schlegel, H. B.; Scuseria, G. E.; Robb, M. A.; Cheeseman, J. R.; Zakrzewski, V. G.; Montgomery, J. A., Jr.; Stratmann, R. E.; Burant, J. C.; Dapprich, S.; Millam, J. M.; Daniels, A. D.; Kudin, K. N.; Strain, M. C.; Farkas, O.; Tomasi, J.; Barone, V.; Cossi, M.; Cammi, R.; Mennucci, B.; Pomelli, C.; Adamo, C.; Clifford, S.; Ochterski, J.; Petersson, G. A.; Ayala, P. Y.; Cui, Q.; Morokuma, K.; Malick, D. K.; Rabuck, A. D.; Raghavachari, K.; Foresman, J. B.; Cioslowski, J.; Ortiz, J. V.; Baboul, A. G.; Stefanov, B. B.; Liu, G.; Liashenko, A.; Piskorz, P.; Komaromi, I.; Gomperts, R.; Martin, R. L.; Fox, D. J.; Keith, T.; Al-Laham, M. A.; Peng, C. Y.; Nanayakkara, A.; Challacombe, M.; Gill, P. M. W.; Johnson, B.; Chen, W.; Wong, M. W.; Andres, J. L.; Gonzalez, C.; Head-Gordon, M.; Replogle, E. S.; Pople, J. A. *Gaussian 98*, Revision A.9; Gaussian, Inc.: Pittsburgh, PA, 1998.

(28) Häberlen, O. D.; Rösch, N. *J. Phys. Chem.* **1993**, *97*, 4970.

(29) Fernández, E. J.; Gimeno, M. C.; Jones, P. G.; Laguna, A.; Laguna, M.; López-de-Luzuriaga, J. M.; Rodriguez, M. A. *Chem. Ber.* **1995**, *128*, 121.

(30) (a) Xia, B.-H.; Zhang, H.-X.; Che, C.-M.; Leung, K.-H.; Philips, D. L.; Zhu, N.; Zhou, Z.-Y. *J. Am. Chem. Soc.* **2003**, *125*, 10362. (b) Yip, H.-K.; Lin, H.-M.; Cheung, K.-K.; Che, C.-M.; Wang, Y. *Inorg. Chem.* **1994**, *33*, 1644. (c) Yip, H.-K.; Lin, H.-M.; Wang, Y.; Che, C.-M. *Inorg. Chem.* **1993**, *32*, 3402.

(31) Møller, C.; Plesset, M. S. *Phys. Rev.* **1934**, *46*, 618.

(32) (a) Foresman, J. B.; Head-Gordon, M.; Pople, J. A.; Frisch, M. J. *J. Phys. Chem.* **1992**, *96*, 135. (b) Raghavachari, K.; Pople, J. A. *Int. J. Quantum Chem.* **1981**, *20*, 1067.

(33) Foresman, J. B.; Frisch, Æ. *Exploring Chemistry with Electronic Structure Methods*, 2nd ed.; Gaussian, Inc.: Pittsburgh, PA, 1996.

(34) (a) van Zyl, W. E.; López-de-Luzuriaga, J. M.; Mohamed, A. A.; Staples, R. J.; Fackler, J. P., Jr. *Inorg. Chem.* **2002**, *41*, 4579. (b) van Zyl, W. E.; López-de-Luzuriaga, J. M.; Fackler, J. P., Jr. *J. Mol. Struct.* **2000**, *516*, 99.

(35) (a) Wadt, W. R.; Hay, P. J. *J. Chem. Phys.* **1985**, *82*, 284. (b) Hay, P. J.; Wadt, W. R. *J. Chem. Phys.* **1985**, *82*, 299.

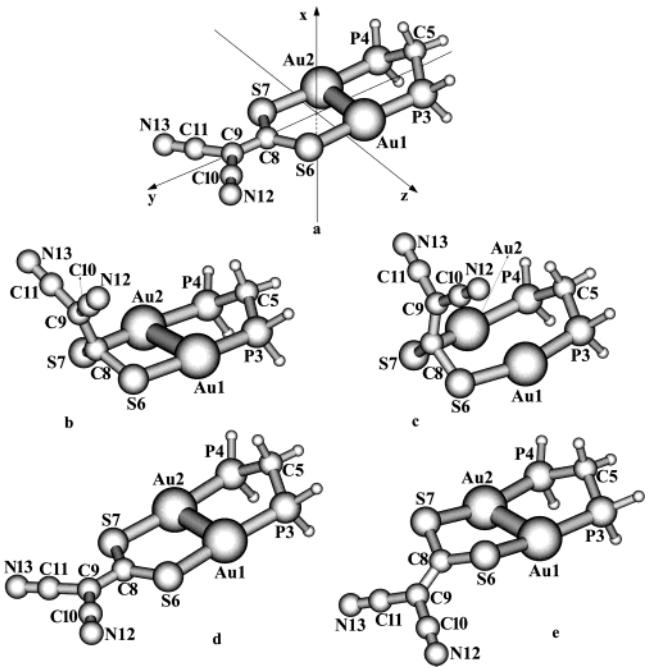

Figure 1. Optimized structures of the $^1A'$ ground state (a) using the MP2 method and the a^3A' (b), b^3A'' (c), c^3A' (d), and $^1A''$ (e) excited states using the CIS method for [Au_2(dpm)(i-mnt)] (**1**).

the calculations. All the calculations are accomplished by using the GAUSSIAN 98 program package[27] on an Origin/3800 server.

III. Results and Discussion

IIIA. Absorption and Emission of the i-mnt Ligand. The structure of the i-mnt ligand in the ground state is fully optimized by the MP2 method. In the calculations, we assume that the ligand also has the same C_s symmetry as that of **1**. The IPCM approach in the SCRF method is employed to simulate the behavior of the i-mnt ligand in the dilute acetonitrile solution. According to the vertical electron transition mechanism in the absorption process, the optimized geometry of the ground state is kept, while the CIS method is performed to calculate the excited state related to the absorption. With respect to the $^1A'$ ground state under the C_s group, both the $^1A' \rightarrow {}^1A'$ and $^1A' \rightarrow {}^1A''$ transitions are dipole-allowed.

By the combination of the CIS and IPCM methods, the absorption is obtained for the i-mnt ligand in acetonitrile. The absorption originating from the $^1A' \rightarrow {}^1A'$ transition is calculated at 268 nm with the oscillator strength of 0.512. In S-Table 2 (Supporting Information) we present the difference of the natural atomic orbital populations for the $^1A'$ ground state and corresponding $^1A'$ excited state. To conveniently compare spectroscopic properties of the i-mnt ligand and **1**, we use the same number to label the atoms of i-mnt for both the i-mnt ligand and **1** as shown in S-Figure 1 (Supporting Information) and Figure 1, respectively. From S-Table 2, the charge mainly transfers from the C9 atom to the C8 atom in the 268 nm absorption. By analyzing the wave functions related to the transition, the absorption is assigned as a $\pi \rightarrow \pi^*$ transition localized on the C=C double bond. To best describe the $^1A' \rightarrow {}^1A'$ transition process, the electron density diagrams of the frontier molecular orbitals of the absorption are displayed in S-Figure 2. The 11a′ orbital (HOMO) has C=C π-bonding character, while the 12a′ orbital (LUMO) is the π^*-antibonding orbital. Gray et al.[22] studied the electronic spectra of a series of metal complexes containing the i-mnt ligand in acetonitrile, and some absorptions ranging from 250 to 350 nm were attributed to L→L* charge-transfer transitions.

The CIS method is used to optimize the excited-state structure of the i-mnt ligand. The phosphorescent emissions at 611 nm in the gas phase and at 714 nm in acetonitrile are obtained, originating from the $^3A' \rightarrow {}^1A'$ transition. The differences between the $^3A'$ excited state and the corresponding $^1A'$ ground state in the natural atomic orbital populations for the two emissions are listed in S-Table 2. Apparently, the change of the orbital populations in the emissive transitions is similar to that of the 268 nm absorption. There is significant charge transfer from the C9 atom to the C8 atom in both the gas phase and solution. However, for the emissive process, the electron should transfer from the excited state to the ground state, i.e., C8→C9 charge transfer. Thus, we assign the emissions as $\pi^* \rightarrow \pi$ transitions involving the carbon double bond just like the transition property of the 268 nm absorption.

IIIB. Ground-State Structure of [Au_2(dpm)(i-mnt)]. The full MP2 optimization on **1** indicates that the complex has a $^1A'$ ground state with the [31(a′^{2})24(a″^{2})] electronic configuration. The corresponding geometry structure is illustrated in Figure 1a, in which the two Au atoms bond with the S and P atoms in the i-mnt and dpm ligands, respectively, forming an eight-membered ring skeleton. The main geometry parameters are listed in Table 1 along with the experimental values of [Au_2(dmpm)(i-mnt)] from X-ray crystal diffraction.[12] The dihedral angles of P3−Au1−Au2−S7, S6−C8−C9−S7, and Au1−S6−S7−C8 are −179.1°, −179.9°, and −179.9°, respectively, indicating that Au, P, and i-mnt are nearly coplanar. The C5 atom lies above the plane with a 136.0° dihedral angle of C5−P4−P3−Au1. The Au(I) atoms take the typical linear two-coordinated geometry,[20a] and the 174.4° P3−Au1−S6 angle agrees well with 175.5° in the crystal from X-ray diffraction. The calculated bond lengths of 2.313 Å for Au−P and 2.333 Å for Au−S are comparable to the reported average values of 2.261 and 2.314 Å, respectively.[12−14]

The Au^I−Au^I separation, 2.913 Å, is in agreement with the experimental 2.909 Å, which is much less than the van der Waals contacts of 3.4 Å.[15] The bite distances of 3.063 Å for P···P and 3.209 Å for S···S are apparently longer than the Au−Au contact; the P3−Au1−Au2 angle of 91.9° and S6−Au1−Au2 angle of 93.6° denote that the two Au(I) atoms tend to approach each other. Such calculated results all suggest that there is weak aurophilic attraction existing between the two Au(I) atoms. We have calculated the frequency of **1** in the $^1A'$ ground state at the MP2 level, to characterize the Au−Au interaction. Through the vibrational mode analysis, the calculated frequency of 110 cm^{-1} is attributed to the Au−Au stretching frequency, which falls well within the range of Au−Au stretching frequencies reported in

Table 1. Optimized Geometry Parameters of the $^1A'$ Ground State under the MP2 Calculations and the a^3A', b^3A'', c^3A', and $^1A''$ Excited States under the CIS Calculations for [Au_2(dpm)(i-mnt)] (1), Together with the Experimental Data for [Au_2(dmpm)(i-mnt)]

	ground state		triplets			singlets
	$^1A'$	exptl	a^3A'	b^3A''	c^3A'	$^1A''$
			Bond Lengths (Å)			
Au1−Au2	2.913	2.909	3.358	3.467	2.920	2.798
Au1−P3	2.313	2.261	2.377	2.405	2.393	2.527
Au1−S6	2.333	2.314	2.387	2.449	2.413	2.462
S6−C8	1.768	1.764	1.760	1.725	1.747	1.748
C8−C9	1.408	1.378	1.497	1.414	1.404	1.378
C9−C10	1.455	1.502	1.422	1.419	1.433	1.433
C10−N12	1.217	1.216	1.158	1.161	1.155	1.155
P3−C5	1.857	1.843	1.845	1.846	1.851	1.852
P3···P4	3.063		3.109	3.122	3.143	3.159
S6···S7	3.209		3.117	2.745	3.198	3.024
			Bond Angles (deg)			
P3−Au1−S6	174.4	175.5	174.1	164.9	174.0	167.1
P3−Au1−Au2	91.9	91.2	87.0	85.9	92.7	94.1
S6−Au1−Au2	93.6	93.4	87.1	81.5	93.3	92.6
P3−C5−P4	111.1	116.3	114.8	115.4	116.3	117.1
S6−C8−S7	130.3	131.0	124.6	105.4	132.6	119.8
			Dihedral Angles (deg)			
C5−P4−P3−Au1	136.0		133.3	129.5	135.8	135.8
P3−Au1−Au2−S7	−179.1		179.4	−171.6	−179.5	−168.9
S6−C8−C9−S7	−179.9		170.0	151.5	179.7	176.8
Au1−S6−S7−C8	−179.9		−115.4	−96.1	179.8	128.4

experiment[7a,36] and calculation.[37] The Au−Au stretching frequency provides the evidence for the weak aurophilic attraction between the two gold(I) atoms. Applying Bruce's empirical equation[8a] about Au−Au interaction energy (D, in kJ/mol),

$$D(\mathrm{Au-Au}) = 1.27 \times 10^6 \mathrm{e}^{-3.5 r_e(\mathrm{Au-Au})}$$

the energy of the Au^I−Au^I aurophilic interaction in **1** is estimated to be about 47 kJ/mol.

The natural population analysis[38] by using the MP2 density shows that the Au atom has a net +0.29 electronic charge, while electronic charges residing on the P and S atoms are +0.45 and −0.22, respectively. The electrons of the S and P atoms transfer to the original 6s and 6p empty orbitals of the Au(I) atoms. Consequently, the closed-shell electronic configuration, $5d^{10}6s^0$, is no longer kept in **1** and is $4f^{0.03}5d^{9.71}6s^{0.88}$-$6p^{0.08}$ instead, just like the case for the previous studies on the Au(I) complexes **2**−**4**.[21] Such a destruction of the closed-shell structure of the Au(I) atom is one of the prominent driving forces to form aurophilic attraction in the Au(I) complexes.

IIIC. Absorption Spectra of [Au_2(dpm)(i-mnt)] in Acetonitrile. The IPCM approach in the SCRF method is employed to interpret the behavior of complex **1** in dilute solution. On the basis of the ground-state geometry, the electronic structures of the excited state and the absorption properties are obtained for **1** in acetonitrile by the combination of the CIS and IPCM methods. We list in Table 2 the three low-lying absorption wavelengths and corresponding oscillator strengths, together with the excitation configurations (|CI coefficient| > 0.2) contributing to these transitions.

Table 2. Calculated Absorptions of [Au_2(dpm)(i-mnt)] (1) in Acetonitrile Solution at the CIS Level, Associated with the Observed Absorptions of [Au_2(dmpm)(i-mnt)] in Acetonitrile

transition	configs	|CI coeff| > 0.2	λ_{calc} (nm)	oscillator strength	λ_{expt} (nm)
$X^1A'\rightarrow A^1A''$	24a″→32a′	0.61059	312	0.091	250−400
	23a″→33a′	−0.23601			
$X^1A'\rightarrow B^1A'$	31a′→33a′	0.61158	300	0.759	
	31a′→34a′	0.28280			
$X^1A'\rightarrow C^1A''$	23a″→33a′	0.59240	279	0.152	
	24a″→32a′	0.22354			

Table 3. Partial Molecular Orbital Compositions (%) of [Au_2(dpm)(i-mnt)] (1) in Acetonitrile under CIS Calculations

MO	energy (eV)	compositions (%) 2Au	dpm	i-mnt	components of orbital
38a′	3.1753	22.1	33.5	44.4	$Au(p_y)$+C8(s)+C5(s)
37a′	3.1165	56.5	19.5	24.0	$Au(p_z)$+C8(s)
27a″	3.1019	84.5	2.7	12.7	$Au(p_y)$
36a′	2.8847	51.8	40.8	7.4	$Au(p_x, p_y)$+$P(p_x)$
35a′	2.4814	42.1	45.5	12.4	$Au(p_y, p_z)$+$P(p_z)$
26a″	1.9693	80.4	9.0	10.7	$Au(p_x, p_z)$
34a′	1.7503	13.6	19.9	66.5	$S(p_x)$+$C8(p_x)$+$C9(p_x)$+$Au(p_x)$
25a″	1.7239	75.0	14.3	10.7	$Au(p_x, p_z)$
33a′	0.0150	21.2	28.3	50.4	$C8(p_x)$+$C9(p_x)$+$Au(p_x)$
32a′ (LUMO)	−0.0433	32.1	49.3	18.6	$Au(p_z)$+$P(p_z)$+C5(s)
31a′ (HOMO)	−8.2487	5.8	0.5	93.7	$S(p_x)$+$C9(p_x)$+$N(p_x)$
24a″	−8.5423	26.8	10.2	62.9	$S(p_y)$+$Au(d_{y^2-z^2})$
23a″	−9.0141	12.3	0.8	86.9	$S(p_x)$+$Au(d_{xy})$
22a″	−9.9298	31.0	47.4	21.6	$P(p_y)$+$Au(p_y)$+$S(p_z)$
30a′	−10.1156	16.8	10.4	72.9	$S(p_y)$+$Au(p_y)$

To assign the absorption in solution, the partial molecular orbital compositions (%) related to the absorption transition are given in Table 3. The coordinate orientation of **1** is depicted in Figure 1a. We also present the differences in natural atomic orbital populations between the ground state and each of the three low-lying excited states in S-Table 3 to aid in the assignment of absorption.

(36) Perreault, D.; Drouin, M.; Michel, A.; Miskowski, V. M.; Schaefer, W. P.; Harvey, P. D. *Inorg. Chem.* **1992**, *31*, 695.
(37) Rawashdeh-Omary, M. A.; Omary, M. A.; Patterson, H. H.; Fackler, J. P., Jr. *J. Am. Chem. Soc.* **2001**, *123*, 11237.
(38) (a) Foster, J. P.; Weinhold, F. *J. Am. Chem. Soc.* **1980**, *102*, 7211. (b) Reed, A. E.; Weinstock, R. B.; Weinhold, F. *J. Chem. Phys.* **1985**, *83*, 735. (c) Reed, A. E.; Curtiss, L. A.; Weinhold, F. *Chem. Rev.* **1988**, *88*, 899.

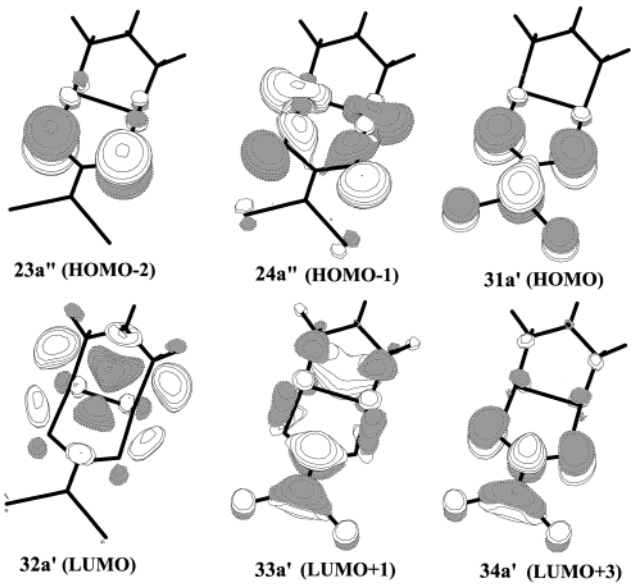

Figure 2. Electron density diagrams of the frontier molecular orbitals involved in the absorption transitions under the CIS calculations for [Au$_2$(dpm)(i-mnt)] (**1**) in acetonitrile.

The calculated lower-energy absorption in acetonitrile is at 312 nm, which originates from the $X^1A' \rightarrow A^1A''$ transition and has the oscillator strength of 0.091. In the excitation, the 24a″→32a′ configuration has the largest coefficient (about 0.61) in the CI wave functions, which is responsible for the absorption. As shown in Table 3, the 24a″ orbital (HOMO−1) has 63% i-mnt ligand composition mainly contributed by the S(p_y) (44%) orbital, while the metal (32%) and dpm ligand (49%) play an important role in the 32a′ orbital (LUMO) mainly from Au(p_z) (29%), C5(s) (22%), and P(p_z) (15%) character. We have displayed in Figure 2 the electron density diagrams of the frontier molecular orbitals involved in the absorption transitions in acetonitrile. The electron density is localized on the S and Au atoms in the 24a″ orbital, but in the 32a′ orbital the electron density is distributed between Au centers and P atoms to form σ(Au$_2$) and σ(P$_2$) bondings, respectively. Combining Table 3 with Figure 2, we attribute the 312 nm absorption to S(p_y)→dpm charge transfer (ligand to ligand charge transfer, LLCT), S(p_y)→Au(p_z) charge transfer (LMCT), and Au($d_{y^2-z^2}$)→Au(p_z) ($d_{\sigma^*} \rightarrow p_\sigma$, metal-centered, MC) transition. The assignment can be further supported by the change of natural orbital populations in the Au, P, and S atoms as shown in S-Table 3. The 3p orbital of the S atom loses 0.24 e; the 6p orbital of Au increases 0.11 e; the 3p orbital of P atom gains 0.09 e. The transition of about 0.06 Au 5d electron to the Au 6p orbital shows that the MC transition exists in the absorption. It is worth noting that the dpm ligand gets a total of 0.27 e, while the i-mnt ligand loses 0.23 e. Thus, the 312 nm $X^1A' \rightarrow A^1A''$ transition mainly has LLCT character.

With respect to the B^1A' excited state, the electronic absorption is calculated at 300 nm with the largest oscillator strength of 0.759 of the three low-lying absorptions, suggestive to be most likely observed in the experiment. As shown in Table 2, the transition is mainly contributed by the 31a′→33a′ and 31a′→34a′ configurations with CI coefficients of about 0.61 and 0.28, respectively. Through Table 3, the 300 nm absorption from the $X^1A' \rightarrow B^1A'$ transition is assigned as an i-mnt intraligand charge transfer (ILCT) with a little LMCT character. The electron density diagrams of the frontier molecular orbitals depicted in Figure 2 can help us intuitively understand the absorption process. The 31a′ orbital (HOMO) has C8−C9 π-bonding properties, but the π* antibondings form between the two carbon atoms in the 33a′ (LUMO+1) and 34a′ (LUMO+3) orbitals. So we further assign the 300 nm absorption to a $\pi \rightarrow \pi^*$ transition involved in the C═C double bond. Comparing the 300 nm absorption of **1** with the 268 nm absorption of the i-mnt ligand, they have the same $^1A' \rightarrow {}^1A'$ transition nature and a similar charge transfer as mentioned above. The 30 nm difference between the two absorption wavelengths is caused by the participation of the metal. Gray et al.[22] studied the electronic spectra of a series of metal complexes containing the i-mnt ligand in acetonitrile, and the absorptions ranging from 250 to 350 nm were attributed to L→L* charge transfer. Our calculated 300 nm absorption arising from the $\pi \rightarrow \pi^*$ transition agrees well with the experiment.

In the calculations, we obtain a second absorption at 279 nm with the most ILCT character. The $X^1A' \rightarrow C^1A''$ transition mainly arises from the combination of 23a″→33a′ (0.59) and 24a″→32a′ (0.22) configurations as seen in Table 2. The 23a″ orbital is the S π orbital from S(p_x), and the 24a″ orbital is mainly composed of S(p_y). However, the π*(C═C), σ(Au$_2$), π(Au$_2$), and σ(P$_2$) components play an important role in the unoccupied 32a′ and 33a′ orbitals. S-Table 3 also gives the quantitative charge transfer by the natural atomic orbital population analyses, where the S 3p orbital loses 0.43 e and the 2p orbitals of the C8 and C9 atoms get 0.25 and 0.09 e, respectively. The i-mnt ligand decreases 0.34 e in all, while the Au centers get 0.21 e. So the 279 nm $X^1A' \rightarrow C^1A''$ transition is unambiguously attributed to S→C8/C9 (ILCT), S→Au (LMCT), and a little Au(d_{xy})→Au(p_x) ($d_{\delta^*} \rightarrow p_\pi$, MC) transitions.

It has been found that the electronic absorptions of [Au$_2$(P−P)(i-mnt)] (P−P = dmpm and dppm) in the acetonitrile solution at room temperature range from 250 to 400 nm, which were experimentally assigned to MC transition interfered with by a strong ILCT transition involving the i-mnt ligand.[12] Apparently, the calculated absorption of **1** reflects the experimental observation and provides more detailed information about transition properties of the absorption.

Compared with the open-ring [Au$_2$(PH$_3$)$_2$(i-mnt)] (**3**) complex,[21c] there are more contribution of P atoms to the absorption process for the closed-ring **1** complex. For example, in the 32a′ (LUMO) orbital of **1** two P(p_z) (16%) orbitals combine into a σ-bonding orbital (Table 3 and Figure 2). The difference is caused by the shorter P···P bite distance in **1** (3.063 Å) than in **3** (3.826 Å).[21c] As a π-conjugated thiolate, the i-mnt ligand plays a dominant role in the absorption process of the Au(I) complex. This has been proved by the calculated 300, 295, and 268 nm absorptions in **1**, **3**, and i-mnt with the larger oscillator strengths of 0.759, 0.765, and 0.512, respectively. In addition, the metal participation in the electronic transitions of **1** and **3** is also important because of the shorter Au^I-Au^I distances (2.913 Å in **1** and 2.945 Å in **3**). In short, just like the absorption with the various

Table 4. Optimized Geometry Parameters of the Triplet Excited States by the UMP2 Method for $[Au_2(dpm)(i\text{-}mnt)]$ (1), $[Au_2(dpm)_2]^{2+}$ (2), $[Au_2(PH_3)_2(i\text{-}mnt)]$ (3), $[Au_2(dpm)(SCH_2S)]$ (4), and $[Au_2(dpm)(SHCH_2SH)]^{2+}$ (5), Together with the Ground-State Results[a]

	1	2	3	4	5
	$^3A'$	^3A_u (^1A_g)[b]	$^3A'$ ($^1A'$)[c]	$^3A''$ ($^1A'$)[d]	$^3A''$ ($^1A'$)[e]
			Bond Lengths (Å)		
Au1−Au2	2.787	2.678 (3.033)	2.786 (2.945)	2.778 (3.011)	2.620 (2.989)
Au1−P3	2.324	2.404 (2.377)	2.356 (2.327)	2.333 (2.318)	2.399 (2.343)
Au1−S6	2.386		2.445 (2.335)	2.388 (2.336)	2.491 (2.422)
S6−C8	1.713		1.723 (1.782)	1.860 (1.867)	1.871 (1.860)
C8−C9	1.488		1.483 (1.406)		
C9−C10	1.454		1.455 (1.455)		
C10−N12	1.147		1.147 (1.216)		
P3−C5	1.869	1.877 (1.874)		1.890 (1.877)	1.878 (1.873)
P3···P4	3.149	3.109 (3.104)	5.264 (3.826)	3.180 (3.062)	3.133 (3.107)
S6···S7	3.156		3.153 (3.223)	2.836 (3.200)	3.273 (3.237)
			Bond Angles (deg)		
P3−Au1−S6	170.4	169.7 (178.3)	144.0 (165.7)	172.3 (176.4)	166.3 (175.4)
P3−Au1−Au2	94.5	95.1 (90.9)	121.8 (100.9)	94.9 (90.6)	96.1 (91.4)
S6−Au1−Au2	94.4		94.3 (93.4)	90.7 (92.3)	97.5 (92.9)
P3−C5−P4	114.8				
S6−C8−S7	134.1		132.4 (129.4)		
			Dihedral Angles (deg)		
P−Au−Au−S/P	−176.5	180.0 (180.0)	180.0 (180.0)	−174.7 (177.9)	−178.7 (−178.7)
S6−C8−C9−S7	179.2		180.0 (−179.4)		
Au1−S6−S7−C8	175.5		−180.0 (−178.1)		
freq (cm^{-1})[f]	135 (110)	144 (89)	119 (96)	126 (93)	164 (96)

[a] Geometry parameters in the ground states are listed in parentheses. [b] Results of **2** from ref 21e. [c] Ground-state results of **3** from ref 21c. [d] Ground-state results of **4** from ref 21b. [e] Results of **5** from ref 21e. [f] Au−Au stretching frequencies.

transition properties mentioned above, complex **1** is expected to have rich emissive properties.

IIID. Excited-State Structures of $[Au_2(dpm)(i\text{-}mnt)]$. To describe the emissive properties of **1**, the CIS method is used to optimize the geometry structure of the excited state, and four excited states with a^3A', b^3A'', c^3A', and $^1A''$ symmetries are obtained. The main geometry parameters of these excited states are presented in Table 1, and their structures are shown in Figures 1b−e. Table 1 and Figure 1 illustrate that the c^3A' excited state still keeps the structure similar to the $^1A'$ ground state, while great changes of the geometry structures occur in other excited states compared to the ground state. Although the $Au_2P_2S_2$ moiety in the a^3A', b^3A'', and $^1A''$ excited states is almost kept coplanar as in the ground state, the other parts of the i-mnt ligand deviate greatly from the $Au_2P_2S_2$ plane (Figure 1). In the a^3A' and b^3A'' states the i-mnt ligand and the C5 atom take the boat conformation; however they adopt the chair conformation in the $^1A''$ singlet excited state. As shown in Table 1, the i-mnt ligand distorts from its original planar structure by 10.0°, 28.5° and 3.2° in the a^3A', b^3A'', and $^1A''$ states, respectively, which is reflected by the calculated dihedral angle of S6−C8−C9−S7. The distortion of the $Au_2P_2S_2$ plane by 8.4° and 11.1° occurs in the b^3A'' and $^1A''$ states, respectively. Of particular interest is the much shorter S···S bite distance of 2.745 Å in the b^3A'' excited state than the bite distances of 3.024−3.198 Å in the other excited states. We conjecture that in the b^3A'' excited state the repulsion of lone-pair electrons on the S atom is reduced greatly because of the charge transfer from the S atoms to the other part of the molecule (Au centers and/or the other atoms of the i-mnt ligand) in the process of electronic transition.

The Au^I−Au^I distances of 3.358 and 3.467 Å for the a^3A' and b^3A'' states, respectively, enlarge dramatically with respect to that (2.913 Å) in the $^1A'$ ground state, indicating that the aurophilic attraction decreases greatly in the excited states. In contrast, the $^1A''$ excited state presents a much shorter Au^I−Au^I distance (2.798 Å). The comparison between the ground state and excited state in the geometry structure can help us predict the emissive properties. For the $^1A''$ singlet excited state, the change of the geometry structure is very similar to that in the ^3A_u excited state of complex **2**, which possesses a much shorter Au^I−Au^I distance of 2.75 Å and a longer Au−P distance of 2.67 Å than 3.17 and 2.45 Å of the ^1A_g ground state, respectively.[21a] This implies that the $^1A''$ excited state may produce similar emission with the MC transition because the promotion of electrons from the d_{σ^*} antibonding orbital to the s_σ and/or p_σ bonding orbital will shorten the Au−Au contact in the $^1A''$ excited state. The a^3A' excited state likely gives rise to the $\pi^*\rightarrow\pi$ transition because of the longer C8−C9 bond distance (1.497 Å) than that (1.408 Å) in the ground state. However, the prediction of the b^3A'' emissive state is not easy. According to the shorter (2.745 Å) S···S bite distance and the longer (2.449 Å) Au−S bond length, we may predict the excited state has Au→S charge-transfer character. Nevertheless, the much longer (3.467 Å) Au^I−Au^I distance opposes the assignment, as the lower-energy unoccupied orbitals contributed by gold centers have the most character of Au−Au bonding from the combination of Au 6s and 6p orbitals, which favors the stronger Au−Au aurophilic attraction and the shorter Au−Au distance. We will solve the dilemma in the following section by comparing with the $^3A''$ excited state of **4**, which produces emission with Au−Au→S charge transfer.

In addition, we use the unrestricted MP2 method to optimize the triplet excited state of **1** to shed some light on the Au−Au bonding properties of the excited state. The optimized main geometry parameters of the $^3A'$ excited state are given in Table 4. The wave functions of the triplet excited state demonstrate that the HOMO

Table 5. Calculated Emissions of [Au$_2$(dpm)(i-mnt)] (1), [Au$_2$(PH$_3$)$_2$(i-mnt)] (3), [Au$_2$(dpm)(SCH$_2$S)] (4), and i-mnt Ligand in the Gas Phase and Solution under the CIS Calculations, Together with the Experimental Results

complex	medium	$a^3A' \rightarrow {}^1A'$	exptl	$b^3A'' \rightarrow {}^1A'$	exptl	$c^3A' \rightarrow {}^1A'$	exptl	$^1A'' \rightarrow {}^1A'$	exptl
1	gas	672		454		307/306[a]		301 (0.030)[b]	
	MeCN	716		624		512	558[c]	375 (0.029)[b]	400[d]
3[e]	gas	593	595[f]			414/450[a]	462[f]		
	$C_2H_2Cl_2$	702				495/531[g]	525[h]		
4[i]	gas			462	500[j]				
	MeCN			510					
i-mnt	gas	611	595[f]						
	MeCN	714							
transition properties									
		$\pi^* \rightarrow \pi$		Au−Au→S		Au−Au→i-mnt		Au($(sp)_\sigma$)→Au(d_{σ^*})	
		^{3}ILCT		^{3}MMLCT		^{3}MMLCT		^{1}MC transition	

[a] Two emissions from monomer and dimer, respectively. [b] Oscillator strength in parentheses. [c] Emission in acetonitrile at 77 K from ref 12. [d] The 400 nm fluorescence of other related Au(I) complexes, [Au$_2$(dmpm)(S$_2$CNEt$_2$)]Cl and [Au$_2$(dppm)(S$_2$CNEt$_2$)](PF$_6$), in the lower-concentration acetonitrile solution at 298 K from ref 12. [e] From the calculated results of ref 21c. [f] The 595 nm emission of K$_2$(i-mnt) and 462 nm emission of [Au$_2$(PPh$_3$)$_2$(i-mnt)] in the solid state at 20 K from ref 10. [g] The 495 nm emission is obtained by the IPCM/CIS method, and the 531 nm emission is from the combination of solid and solvent effects, comparable to the experimental emission in solution at lower temperature. [h] The emission in actonitrile at 77 K from ref 18. [i] From the calculated results of ref 21b. [j] The solid-state emission from ref 8b.

is the σ-bonding orbital mainly contributed by the Au(p_z) atomic orbitals and the LUMO comes from the i-mnt ligand. The ^{3}A′ excited state in the UMP2 calculations has orbital character very similar to those of the c^3A′ excited state in the CIS calculations. Apparently, the triplet excited state in the UMP2 calculations corresponds to the c^3A′ excited state in the CIS calculations because of the similar excited-state wave functions, the same ^{3}A′ excited-state symmetry, and the similar geometry structures as shown in Tables 1 and 4. Compared with those of the c^3A′ excited state optimized by the CIS method, the geometry parameters of the ^{3}A′ excited state by the UMP2 method are more unrelaxed. This is just because the latter includes more electron correlation effects.[4a−e] The Au−Au distance calculated by UMP2 are 0.133 Å shorter than by CIS, while the differences of other distances are very small (<0.08 Å).

Table 4 also presents the optimized ground- and excited-state geometry parameters of **2**−**5** using the MP2 and UMP2 methods.[21b,c,e] Compared with those of the ground states of **1**−**5** under the MP2 calculations as shown in Tables 1 and 4, the Au−Au distances of the triplet excited states shorten about 0.13−0.37 Å, while the Au−P/S bond lengths elongate about 0.01/0.03−0.06/0.11 Å. Analyses on the wave functions of the triplet excited states indicate that the promotion of electrons from the i-mnt ligand (**1** and **3**), d_{σ^*} (**2** and **5**), and the lone pair electrons of the S atoms (**4**) orbitals to s_σ and/or p_σ orbitals of Au centers results in the formation of an Au−Au σ bond in the excited states. The enhancement of the Au−Au aurophilic attraction naturally weakens the bonding between the Au and P/S atoms.

Frequency calculations have been performed on **1**−**5** at the MP2 level for the triplet excited state. The calculated Au−Au stretching frequencies (Table 4) fall well within the range of the experiment[7a,36,39,40] and calculations.[21c,e,37,41] The 119−164 cm^{-1} Au−Au stretching frequency of the excited state agrees well with experimental Au(II)−Au(II) frequencies of 105, 125, and 157 cm^{-1} for [Au$_2$X$_2$(CH$_2$PPh$_2$S)$_2$][39] and 103, 132, and 162 cm^{-1} for [Au$_2$X$_2$(CH$_2$PPh$_2$CH$_2$)$_2$][39,40] (X = I, Br, and Cl), respectively. The present calculations suggest that the Au−Au interaction is weak in the ground state (mean 2.95 Å Au−Au distance and 95 cm^{-1} Au−Au stretching frequency), but is strongly enhanced in the triplet excited state (mean 2.70 Å Au−Au distance and 140 cm^{-1} Au−Au stretching frequency). Table 4 demonstrates the Au−Au stretching frequency is correlated with the Au−Au distance, namely, stronger frequency, shorter distance.

IIIE. Emission Spectra of [Au$_2$(dpm)(i-mnt)] and Related Au(I) Complexes. Under the CIS calculations, four emissions are obtained at 672, 454, 307, and 301 nm in the gas phase corresponding to the a^3A′, b^3A″, c^3A′, and ^{1}A″ excited states, respectively (Table 5). To conveniently discuss the transition property of emission, we present the natural atomic orbital populations of the excited state and the corresponding ground state in Table 6. On the basis of the optimized excited-state structures of **1**, the IPCM method[25−27] is employed to account for the solvent effect of acetonitrile. The emissions in dilute acetonitrile solution are calculated at 716, 624, 512, and 375 nm, produced by these four excited states, respectively.

The calculated lowest-energy emission occurs at 672 nm in the gas phase with the nature of $a^3A' \rightarrow {}^1A'$ transition. One can see from Table 6 that the differences of Au centers, i-mnt, and dpm between the a^3A′ excited state and the corresponding ^{1}A′ ground state in the natural orbital populations are very small (−0.06, 0.07, and −0.01, respectively), indicating the 672 nm transition mainly takes place inside Au centers, i-mnt, and dpm. (The negative value denotes the decrease of orbital population in the electronic transition from excited state to ground state.) Apparently, the change of populations inside the i-mnt ligand plays a significant role in the transition, as in the emissive process the 2p orbital of the C8 atom loses 0.29 e and the 2p orbital of the C9 atom increases 0.36 e. Through analyzing the wave functions of the a^3A′ excited state, we attribute the 672 nm phosphorescent emission to a $\pi^* \rightarrow \pi$ charge transfer (i-mnt ^{3}ILCT) transition involved in the C=C double

(39) Carlson, T. F.; Fackler, J. P., Jr. *J. Organomet. Chem.* **2000**, *596*, 237.
(40) Clark, R. J. H.; Tocher, J. H.; Fackler, J. P., Jr.; Neira, R.; Murray, H. H.; Knachel, H. J. *J. Organomet. Chem.* **1986**, *303*, 437.
(41) Rawashdeh-Omary, M. A.; Omary, M. A.; Patterson, H. H.; Fackler, J. P., Jr. *J. Am. Chem. Soc.* **2001**, *123*, 11237.

Table 6. Natural Atomic Orbital Populations of the a^3A', b^3A'', c^3A', and $^1A''$ Excited States and Their Corresponding $^1A'$ Ground States for the 672, 454, 307, and 301 nm Emissions of [Au_2(dpm)(i-mnt)] (1) under the CIS Calculations, Respectively

atom	orbital	$^1A'$	a^3A'	$^1A'$	b^3A''	$^1A'$	c^3A'	$^1A'$	$^1A''$
Au	6s	0.736	0.762	0.703	0.834	0.749	0.828	0.731	0.782
	6p	0.027	0.028	0.026	0.031	0.029	0.157	0.032	0.140
	5d	9.808	9.809	9.820	9.820	9.812	9.810	9.817	9.659
	4f	0.006	0.006	0.005	0.006	0.006	0.007	0.006	0.008
P	3s	1.324	1.326	1.326	1.336	1.333	1.341	1.325	1.311
	3p	3.096	3.098	3.101	3.111	3.093	3.185	3.104	3.115
	3d	0.052	0.052	0.051	0.051	0.051	0.052	0.053	0.056
C5	2s	1.218	1.218	1.219	1.219	1.219	1.240	1.219	1.237
	2p	3.809	3.810	3.809	3.809	3.807	3.807	3.811	3.818
S	3s	1.703	1.713	1.704	1.721	1.700	1.701	1.716	1.717
	3p	4.597	4.576	4.611	4.108	4.556	4.379	4.587	4.460
	3d	0.022	0.024	0.022	0.030	0.022	0.024	0.017	0.016
C8	2s	1.105	1.118	1.066	1.096	1.062	1.116	1.056	1.068
	2p	3.089	3.382	3.118	3.494	3.135	3.162	3.127	3.208
C9	2s	0.927	0.928	0.910	0.905	0.903	0.903	0.907	0.906
	2p	3.422	3.065	3.457	3.599	3.477	3.156	3.454	3.487
C10	2s	0.840	0.856	0.844	0.842	0.845	0.852	0.844	0.844
	2p	2.810	2.850	2.800	2.810	2.805	2.827	2.799	2.803
N	2s	1.598	1.599	1.600	1.599	1.595	1.595	1.597	1.597
	2p	3.797	3.739	3.798	3.843	3.804	3.735	3.794	3.805
Δ(2Au)[a]		−0.056		−0.274		−0.412		−0.006	
Δ(i-mnt)[a]		0.069		0.309		0.668		0.099	
Δ(dpm)[a]		−0.009		−0.041		−0.254		−0.095	

[a] The differences of Au centers, i-mnt, and dpm between the ground and excited states in the natural orbital populations. The negative value denotes the decrease of orbital population in the electronic transition from the excited state to the ground state.

bond from the excited state to the ground state. On the basis of the optimized a^3A' excited state, the 716 nm phosphorescence in acetonitrile is calculated by the CIS/IPCM method, which also has i-mnt ILCT character.

Since the i-mnt ligand is greatly involved in the luminescence of complex **1**, we list in Table 5 the calculated results of **3** and the i-mnt ligand, which both include the same type of $\pi^* \rightarrow \pi$ phosphorescence. In the gas phase, there is about 60−80 nm difference between **1** and **3**/i-mnt in the lowest-energy emission. This is strongly related to the metal participation. In the previous studies,[21c] the calculated geometry parameters of the lowest-energy $^3A'$ excited state of **3** were similar to those of the a^3A' excited state of **1** except for the much longer Au−Au distance (4.753 Å). Such a long Au−Au distance greatly decreases the Au contribution to the lowest-energy transition for complex **3**, so the 593 nm emission of **3** is closer to the 611 nm emission of i-mnt than the 672 nm emission of **1**. It was found that the K_2(i-mnt) complex exhibits an intense phosphorescence of 595 nm in the solid state at 20 K.[10] We have proved in the previous study[21c] that the intermolecular interactions slightly affect the emission. Therefore, the lowest-energy emission in the gas phase may be comparable to the experimental result. In dilute solution, the lowest-energy phosphorescent emissions of **1**, **3**, and i-mnt are calculated at 716, 702, and 714 nm, respectively. The close emission wavelengths result from the fact that the solvent greatly weakens the perturbation of Au centers in the transitions.

For the $b^3A'' \rightarrow {}^1A'$ transition of **1**, the phosphorescence under the CIS calculations in the gas phase and acetonitrile is at 454 and 624 nm, respectively. Table 6 shows in the 454 nm $b^3A'' \rightarrow {}^1A'$ electronic transition that the i-mnt ligand gets a total of 0.31 e and the Au centers lose 0.27 e; however, the population on the dpm ligand is kept unchanged (−0.04 e). Namely, the 454 nm emission has the admixture of Au→S charge transfer (MLCT) and i-mnt ILCT transitions. In S-Table 5, we present the components of the orbitals involved in the emissive transitions. The emission from the $b^3A'' \rightarrow {}^1A'$ transition either in the gas phase or in solution is assigned as an [Au(s, p_y, p_z)+C8(p_x)+C9(p_x)]→S(p_y, p_z) charge transfer; furthermore the σ and/or π Au−Au bonding character in the unoccupied 32−34a′ orbitals indicates that the emission has Au−Au→S charge-transfer (^{3}MMLCT) character. The assignment is clearly conflicted with the calculated much longer Au−Au distance (3.467 Å) in the b^3A'' excited state (Table 1), because the promotion of electrons into the Au−Au bonding orbitals strengthens the Au−Au interaction in the excited state, which is supported by our recent studies on the luminescence and aurophilic attraction of the **4** complex.[21b] The $^3A''$ excited state of **4** gives rise to the 462 nm emission with the nature of Au−Au→S charge transfer (^{3}MMLCT) in the gas phase (Table 5). The Au−Au distance greatly shortens from 3.01 Å in the $^1A'$ ground state to 2.88 Å in the $^3A''$ excited state.

The investigations on a series of binuclear d^8−d^8 complexes[42−46] enlighten us to solve the above contradiction from the ^{3}MMLCT emissive states of complexes **1** and **4**. The determined Pt^{II}−Pt^{II} distances by X-ray crystal diffraction are 3.44, 3.34, and 3.25 Å for [Pt_2-(C≡CR)$_4$(dppm)$_2$] (R = Ph, C_6H_4-Cl-*p*, and C_6H_4-NO_2-*p*), respectively.[42−45] This implies that the shorter Pt^{II}−Pt^{II} distances are found for less electron-rich alkynyl groups. The weaker donor strength of the less electron-rich alkynyl ligands will reduce electron density on the Pt d_{σ^*} antibonding orbital and further pull the platinum centers closer. Cotton et al.[46] also put forward a similar suggestion to explain the modest decrease (0.07 Å) in

(42) Wong, K. M.-C.; Hui, C.-K.; Yu, K.-L.; Yam, V. W.-W. *Coord. Chem. Rev.* **2002**, *229*, 123.
(43) Hui, C.-K.; Chu, B. W.-K.; Zhu, N.; Yam, V. W.-W. *Inorg. Chem.* **2002**, *41*, 6178.
(44) Yam, V. W.-W.; Yu, K.-L.; Wong, K. M.-C.; Cheung, K.-K. *Organometallics* **2001**, *20*, 721.
(45) Yam, V. W.-W.; Hui, C.-K.; Wong, K. M.-C.; Zhu, N.; Cheung, K.-K. *Organometallics* **2002**, *21*, 4326.

Table 7. Compositions (%) of the Frontier Molecular Orbitals Involved in the c^{3}A′→^{1}A′ Transition in the Gas Phase and Acetonitrile Solution for [Au$_2$(dpm)(i-mnt)] (1) under the CIS Calculations

			compositions (%)			
	MO	energy (eV)	2Au	dpm	i-mnt	components of orbital
in gas phase	40a′	4.9811	13.5	33.4	53.1	C8(s)+C9(p_y)+P(s)+Au(p_x, p_y, p_z)
	38a′	3.1089	9.1	85.9	5.0	P(s, p_z)+C5(s, p_y)
	36a′	2.6556	51.7	38.3	10.0	Au(s, p_x, p_y)+P(p_y)
	32a′ (LUMO)	0.0204	26.5	68.5	5.0	Au(p_z)+P(p_z)+C5(s)
	31a′ (HOMO)	−7.6544	3.0	0.2	96.8	C9(p_x)+S(p_x)+N(p_x)
	29a′	−11.7081	10.7	0.4	88.9	S(p_x)+C8(p_x)+C10(p_x)+N(p_x)+Au(d_{xy})
in acetonitrile	34a′	1.9271	15.5	16.3	68.3	S(p_x)+C8(p_x)+ Au(p_x)
	33a′	0.3255	24.8	22.0	53.2	Au(p_x, p_z)+C8(p_x)+C9(p_x)
	32a′ (LUMO)	0.1791	30.9	47.8	21.4	Au(p_z)+P(p_z)
	31a′ (HOMO)	−8.1923	4.7	0.3	95.0	S(p_x)+C9(p_x)+N(p_x)

the Ni^{II}−Ni^{II} distance on going from Ni$_2$(form)$_4$ to [Ni$_2$(form)$_4$]$^+$ (form = (*p*-CH$_3$C$_6$H$_4$)NCHN(*p*-CH$_3$C$_6$H$_4$)) by the SCF-Xα-SW calculations because of the reduced electron density on the Ni d_{δ^*} antibonding orbital of the latter complex. Since the lesser electron density on the antibonding orbitals favors the stronger metal−metal interaction as mentioned above, conversely the lesser electron density on the bonding orbitals must result in the weaker metal−metal interaction. By carefully inspecting the Au−Au bonding orbitals contributing to the 454 nm b^{3}A″→^{1}A′ transition of **1**, we find that there are clear $\sigma-\pi$ and $\pi-\pi$ interactions in the 33a′ and 34a′ orbitals of the b^{3}A″ excited state, respectively, as shown in Figure 3. The 33a′ orbital is formed by the interaction of the Au−Au σ-bonding orbital and the i-mnt π orbital, while the 34a′ orbital is the combination of the Au−Au π-bonding orbital and the i-mnt π orbital. Such $\sigma-\pi$ and $\pi-\pi$ interactions significantly decrease the electron density in the Au−Au bonding orbitals and naturally result in the much longer Au−Au distance in the b^{3}A″ excited state (3.467 Å) with respect to that in the ^{1}A′ ground state (2.913 Å). In addition, the interactions also interpret the great distortions of the Au1−S6−S7−C8 dihedral angle of −96.1° in the excited state from the original −179.9° in the ground state (Table 1).

The third phosphorescence is calculated at 307 nm arising from the c^{3}A′→^{1}A′ transition in the gas phase. The combination of Tables 6 and 7 shows that the emission has Au−Au→i-mnt charge transfer (^{3}MMLCT) and dpm→i-mnt charge transfer (^{3}LLCT) character. The electron density diagrams of the molecular frontier orbitals for the 307 nm emission in Figure 4 provide intuitive evidence for the above assignment. The electron density mainly focuses around the i-mnt ligand in the 29a′ (HOMO−5) and 31a′ (HOMO) orbitals, which are composed of [π(S−C)+π(C≡N)] and [π(S)+π(C=C)+π(N)], respectively. However the electron density transfers to Au centers and the dpm ligand in 32a′ (LUMO) and 36a′ (LUMO+6) to form the σ(Au$_2$) and σ(P$_2$) orbitals, respectively. The promotion of electrons from the i-mnt ligand orbitals to s_σ and p_σ orbitals of the Au centers results in the formation of an Au−Au σ bond in the c^{3}A′ excited state. The UMP2 calculations on **1** present a ^{3}A′ triplet excited state, possessing HOMO and LUMO character similar to those of the c^{3}A′ excited state in such CIS calculations.

We also list in Table 5 the similar transition of the 414 nm of **3**, which has Au−Au→i-mnt transition properties.[21c] As the phosphine ligand which is combined into relatively higher-energy unoccupied orbitals as reflected in Figure 4, Table 7, and ref 21c has more contribution to the 307 nm transition in **1** than to the 414 nm in **3**, the former has larger emissive energy (4.04 eV, 307 nm). Previously,[21c] the calculations on [Au$_2$(PH$_3$)$_2$(i-mnt)]$_2$ (**3**···**3**) that was used to model the behavior of **3** in the solid state showed that the intermolecular Au−Au interaction strongly affects the emission, causing a ca. 40 nm red shift with respect to

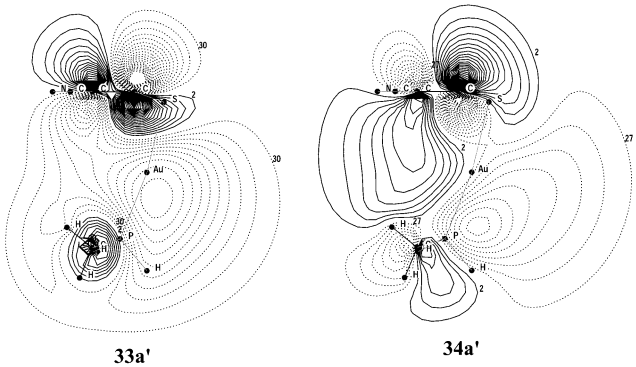

Figure 3. Contour plots of the Au−Au bonding 33a′ (LUMO+1) and 34a′ (LUMO+3) orbitals of the b^{3}A″ excited state of [Au$_2$(dpm)(i-mnt)] (**1**) in the gas phase, showing the $\sigma-\pi$ and $\pi-\pi$ interactions between the electron densities around Au−Au bonding and i-mnt π orbitals.

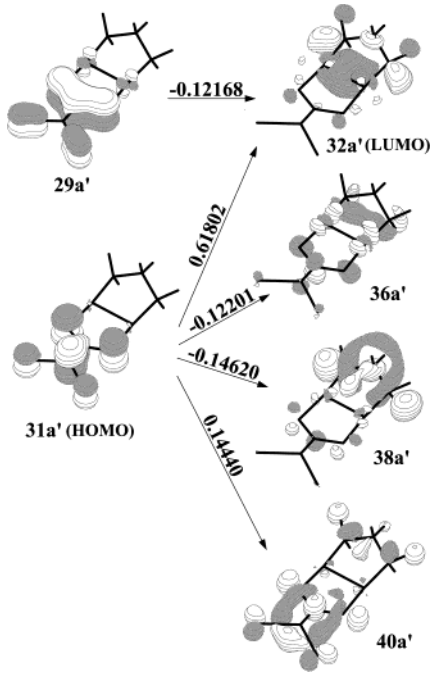

Figure 4. Single electron transitions with |CI coefficient| > 0.1 in the CIS calculations for the 307 nm c^{3}A′→^{1}A′ phosphorescence of [Au$_2$(dpm)(i-mnt)] (**1**) in the gas phase.

the 414 nm emission of **3**, as seen in Table 5. In the crystal, the **1** complex forms a polymeric chain through the significant intermolecular Au−Au interactions between the adjacent molecules.[12] Since the $c^3A'\rightarrow{}^1A'$ transitions of **1** (307 nm) and **3** (414 nm) have similar ^{3}MMLCT character, the intermolecular Au−Au interaction in $[Au_2(dpm)(i\text{-}mnt)]_2$ (**1···1**) may affect the emission of **1** just like the case for **3**. On the basis of the optimized c^3A' excited-state structure of **1**, **1···1** is used to simulate the solid effect of the Au(I) complex in the crystal and further to reveal the influence due to the solid effect on the luminescence of the complex. The intermolecular Au−Au separation changes from 3 to 10 Å with keeping four Au atoms collinear and considering the least steric hindrance. The calculated emission is almost unchanged, ranging from 302 to 307 nm (S-Table 5), which agrees with Tang et al.'s experiment.[12] They have pointed out that although the $[Au_2(dmpm)(i\text{-}mnt)]$ complex is concentration dependent, the shift of emission of the Au(I) complex is not sensitive to dimerization. Therefore, the calculated and experimental results both indicate that the solid effect between two **1** molecules slightly changes the emission spectrum and the single molecule of **1** can be used to describe the behavior of the Au(I) complex in the solid state. So far, the experiments on the $[Au_2(dmpm)(i\text{-}mnt)]$ and $[Au_2(dppm)(i\text{-}mnt)]$ complexes have not shown the emissive bands in the visible region in the solid state, which supports our calculated results.[12]

In fact, many investigations have shown that the intermolecular Au−Au interaction in the Au(I) complexes will affect the solid-state emission with the ^{3}MMLCT character.[1,8,21,34] The interaction between adjacent molecules causes destabilization of the HOMO (i-mnt) and stabilization of the LUMO ($\sigma(Au_2)$), leading to the net effect of the reduced emissive energy. For the pure ^{3}MMLCT emissive excited state of **3**, the red shift of about 40 nm from the solid effect is, indeed, found in **3···3**, as shown in Table 5.[21c] However, the 307 nm emission of **1** possesses ^{3}MMLCT and ^{3}LLCT character, and both characteristics contribute to the solid-state emission. On one hand, the ^{3}MMLCT character in the solid-state emission results in less emissive energy. On the other hand, the approach of two adjacent molecules strongly increases the phosphine−phosphine interaction and the contribution of the phoshine ligand to the emissive transition, especially for **1** (see LUMO in S-Figure 3). As mentioned above, the phosphine ligand occupies relatively higher-energy unfilled orbitals, and more phosphine ligand participation will result in the larger emissive energy. Thus, the solid effect in **1···1** changes the emissive energy in the opposite direction, leading to the unchanged emission wavelength.

As mentioned in the computational details, both solvent and solid effects have to be considered in the calculations to describe the behavior of the emission in solution at lower temperature. Since the solid effect in complex **1** slightly changes the emission, we only take the solvent effect into account to interpret the experimental 558 nm emission of $[Au_2(dmpm)(i\text{-}mnt)]$ observed in acetonitrile at 77 K.[12] Under the IPCM/CIS calculations, the c^3A' excited state produces a 512 nm (2.42 eV) emission in acetonitrile solution, comparable to the experimental 558 nm (2.22 eV) emission, which was experimentally assigned as the Au→i-mnt charge-transfer (^{3}MLCT) transition.[12] The shorter emission wavelength in the calculation with respect to experimental observation is because the CIS method usually overestimates the transition energy.[23,32,47] Table 7 gives the components of the frontier molecular orbitals related to the $c^3A'\rightarrow{}^1A'$ transition in both the gas phase and acetonitrile. The analysis of the table shows that the emissions in the gas phase (307 nm) and solution (512 nm) both have ^{3}MMLCT and ^{3}LLCT character. With respect to the 307 nm emission in the gas phase, the solvent effect of acetonitrile results in a ca. 200 nm red shift. The lesser participation of the dpm ligand in unoccupied oribtals in solution than in the gas phase is one of the important reasons that lead to such a red shift. For **3**, the solvent effect also causes a large red shift (80 nm) of the emission in dilute solution (495 nm) relative to that in the gas phase (414 nm), corresponding to the $c^3A'\rightarrow{}^1A'$ transition of **1**, as seen in Table 5. The solid effect from the intermolecular Au−Au interaction in **3···3** causes a ca. 40 nm red shift with respect to the 414 nm emission of the single **3** molecule. So the combination of both solvent and solid effects in complex **3** gives the 531 nm emission, which agrees well with the experimental 525 nm emission in solution at 77 K.[18] It has been well established that the Au−Au interactions are strongly related to the temperature.[21c,34] Thus, it is reasonable that the solvent effect and solid effect are both considered in the calculations in order to model the emission in the lower temperature solution.

The fluorescence originating from the $^1A''\rightarrow{}^1A'$ transition is calculated at 301 and 375 nm in the gas phase and the dilute acetonitrile solution, respectively, using the same methods as mentioned above. The emissions are attributed to a $Au(s,p_z)\rightarrow Au(d_{z^2},d_{y^2-z^2})$ ($(sp)_\sigma\rightarrow d_{\sigma^*}$, ^{1}MC) transition perturbed by some dpm→S and Au→S charge transfer, which is supported by Table 6 and S-Table 6. The electron density diagrams of the frontier molecular orbitals in Figure 5 provide deep insight into the 301 nm transition process. Tang et al. reported[12] that complexes $[Au_2(dmpm)(S_2CNEt_2)]Cl$ and $[Au_2(dppm)(S_2CNEt_2)](PF_6)$ exhibit fluorescence with the ^{1}MC transition at 400 nm in the lower concentration acetonitrile solution at 298 K, which is similar to our calculated 375 nm emission.

IV. Conclusion

The present calculations on **1** reveal its excited-state properties in the gas phase, solid state, and solution. The luminescence of **1** arising from the a^3A', b^3A'', c^3A', and $^1A''$ excited states includes all the possible transition properties of Au(I) complexes, ranging from ILCT (^{3}ILCT corresponding to the a^3A' excited state), to MLCT (^{3}MMLCT to the b^3A'' and c^3A' states), to MC transition (^{1}MC to the $^1A''$ state), so **1** and its solvated and solid models span an ideal theoretical reference system that can be used to compare the excited-state properties of

(46) Cotton, F. A.; Matusz, M.; Poli, R.; Feng, X. *J. Am. Chem. Soc.* **1988**, *110*, 1144.

(47) (a) Casida, M. E.; Jamorski, C.; Casida, K. C.; Salahub, D. R. *J. Chem. Phys.* **1998**, *108*, 4439. (b) Stratmann, R. E.; Scuseria, G. E. *J. Chem. Phys.* **1998**, *109*, 8218. (c) Bauernschmitt, R.; Ahlrichs, R. *Chem. Phys. Lett.* **1996**, *256*, 454. (d) Matsuzawa, N. N.; Ishitani, A.; Dixon, D. A.; Uda, T. *J. Phys. Chem.* **2001**, *A105*, 4953.

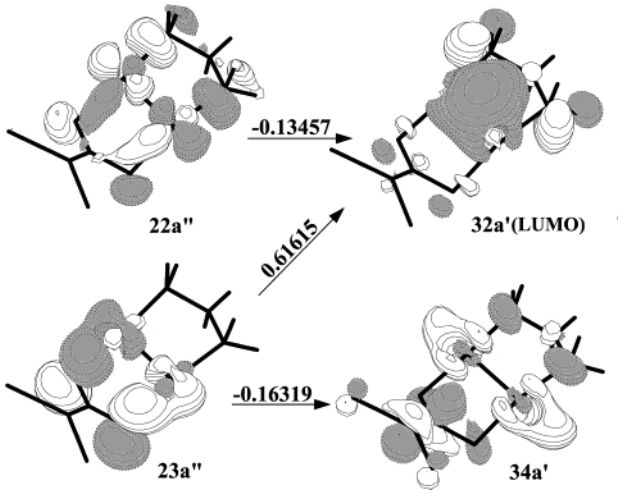

Figure 5. Single electron transitions with |CI coefficient| > 0.1 in the CIS calculations for the 301 nm $^1A''\rightarrow{}^1A'$ fluorescence of [Au$_2$(dpm)(i-mnt)] (**1**) in the gas phase.

many Au(I) complexes. We summarize in Table 5 the detailed results of **1** and related Au(I) complexes on emissions in different media, transition properties, and experimental results.

The π-conjugated i-mnt ligand is greatly involved in electronic transitions for the Au(I) complexes containing such a ligand. For instance, the lowest-energy emission and the absorption with the larger oscillator strength of **1** and **3** have i-mnt ILCT character, and in these transitions the electron density is mainly localized on the i-mnt ligand.[21c]

Usually, the promotion of electrons to the Au−Au bonding orbitals will result in a stronger Au−Au interaction in the excited state[21] just as the $^1A''$ singlet excited state of **1** presents a shorter (2.798 Å) Au−Au distance than the 2.913 Å distance in the $^1A'$ ground state. In contrast, although there is significant charge transfer into the Au−Au bonding orbitals of the b^3A'' excited state of **1**, the calculated Au−Au distance in the excited state elongates about 0.554 Å with respect to that in the ground state. This is because the $\sigma-\pi$ and $\pi-\pi$ interactions between the Au−Au σ/π bonding orbitals and the i-mnt π orbital strongly reduce the electron density around the Au−Au bonding orbitals.

In addition, both solvent effect and solid effect are considered in the calculations in order to model the experimental fluid emission for Au(I) complexes at lower temperature. The studies on the $c^3A'\rightarrow{}^1A'$ transitions of **1** and **3** provide a satisfactory example for the above suggestion.

Finally, systematic studies on a series of Au(I) complexes[21] are necessary to extend the application of the theoretical methods in the transition metal complexes and to provide theoretical support for experimental observations, especially for the existing and/or potential applications of Au(I) complexes.[1,7,9a,24]

Acknowledgment. This work is supported by the Natural Science Foundation of China (20173021, 20333050).

Supporting Information Available: Tables of optimized ground-state geometries of **1** and triplet excited-state geometries of **1**−**5**. Tables of natural atomic orbital populations for the i-mnt ligand and **1** in the acetonitrile solution. Tables of molecular orbital contributions to $a^3A'\rightarrow{}^1A'$, $b^3A''\rightarrow{}^1A'$, and $^1A''\rightarrow{}^1A'$ transitions of **1**. Figures of geometry structure of the i-mnt ligand and electron density diagrams of the i-mnt ligand and the dimer **1**···**1**. This material is available free of charge via the Internet at http://pubs.acs.org.

OM0498652